Non-iterative Market Participation of Virtual Power Plants via Bidding Function Representation

Yiyang Song, Jianxiao Wang, and Yi Wang

***Abstract*—Virtual power plants (VPPs) promote the high-level integration of distributed energy resources (DERs) through complementation and aggregation. To avoid the privacy leakage and enhance the market efficiency, this study aims to achieve the non-iterative market participation of VPPs by accurately characterizing their external bidding functions. To this end, an improved multi-parametric linear programming (MPLP) method is developed to derive the bidding function representation of VPPs. The proposed method projects the detailed internal model of VPPs onto the point of common coupling (PCC). An algorithm for determining a precise initial parameter space (IPS) is proposed, thereby avoiding the redundant solutions that typically occur in traditional MPLP method. The IPS is then partitioned into several critical regions (CRs), within each of which the marginal cost remains constant, facilitating a piecewise linear mapping between the trading power and bidding price. Case studies on modified IEEE 33-bus and IEEE 123-bus systems demonstrate that the proposed method accurately characterizes the bidding functions of VPPs and substantially improves the efficiency of their non-iterative market participation while ensuring data privacy.**

***Index Terms*—Virtual power plant (VPP), bidding function, critical region, electricity market, data privacy, distributed energy resource (RES), multi-parametric linear programming (MPLP).**

Nomenclature

A. Indices and Sets

ϕ^{BS}	Set of energy storage units
ϕ^{D}	Set of loads
ϕ^{MT}	Set of micro-turbine (MT) units
ϕ^{N}	Set of nodes
ϕ^{RG}	Set of renewable energy units
ϕ^{PCC}	Set of points of common coupling (PCCs)
ϕ^{T}	Set of time periods
a, na	Indices of active and nonactive constraints
c	Index of PCCs
d	Index of loads
i	Index of MT units
j	Index of renewable energy units
k	Index of energy storage units
l, n	Index of nodes
r	Index of critical region (CR) boundaries
s	Index of CRs from 0 to S
t	Index of time from 0 to T

B. Parameters and Constants

$\varepsilon_k^{\mathrm{cha}}$	Charging efficiency of energy storage unit k
$\varepsilon_k^{\mathrm{dis}}$	Discharging efficiency of energy storage unit k
$\boldsymbol{\eta}$	Cost coefficient vector of MT unit
$\rho_{l,\max}$	The maximum voltage phase angle of node l
$\rho_{l,\min}$	The minimum voltage phase angle of node l
b_{lc}, g_{lc}	Susceptance and conductance of line lc
$E_{k,\max}$	The maximum capacity of energy storage unit k
$E_{k,\min}$	The minimum capacity of energy storage unit k
$\boldsymbol{I}, \mathbf{1}$	Unit matrix and vector of appropriate dimensions
$\boldsymbol{K}_0, \boldsymbol{k}_0$	Coefficient and constant matrices of initial parameter space
m	Maintenance and operating cost of energy storage unit
M	A large constant
$p_{i,\max}^{\mathrm{MT}}$	The maximum active power output of MT unit i
$p_{i,\min}^{\mathrm{MT}}$	The minimum active power output of MT unit i
$p_{k,\max}^{\mathrm{BS}}$	The maximum charging/discharging power of energy storage unit k
r_i^{MT}	Ramping limit of MT unit i
S_{lc}^{line}	Power flow limit of line lc
$V_{n,\max}, V_{n,\min}$	The maximum and minimum values of square of voltage amplitude at node n

C. Variables

$\boldsymbol{\alpha}_k=[\alpha_{k,1}, \alpha_{k,2}]$	Vector of Lagrange multipliers corresponding to capacity constraints of energy storage unit k

Manuscript received: June 22, 2025; revised: September 15, 2025; accepted: November 11, 2025. Date of CrossCheck: November 11, 2025. Date of online publication: December 29, 2025.

This work was supported by National Key Research and Development Program (No. 2022YFB2405600).

Y. Song and J. Wang (corresponding author) are with the National Engineering Laboratory for Big Data Analysis and Applications, Peking University, Beijing 100871, China (e-mail: yysongol@connect.hku.hk; wang-jx@pku.edu.cn).

Y. Wang is with the Department of Electrical and Electronic Engineering, University of Hong Kong, Hong Kong, China (e-mail: yiwang@eee.hku.hk).

DOI: 10.35833/MPCE.2025.000570

$\rho_{l,t}$	Voltage phase angle of node l at time t
λ_c, λ_n	Lagrange multipliers at PCC c and node n
$\boldsymbol{\theta}$	Amount of electricity interaction between virtual power plants (VPPs) and main grid
$\boldsymbol{\mu}_k=[\mu_{k,m}(t)]$	Vector of Lagrange multipliers corresponding to upper/lower limits on discharging/charging power of energy storage unit k
$\boldsymbol{\varphi}$	Vector of binary variables with same dimension of $\boldsymbol{k}_0$
$\boldsymbol{A}$, $\boldsymbol{B}$	Coefficient matrices corresponding to $\boldsymbol{x}$ and $\boldsymbol{y}$
$\boldsymbol{b}$	Matrix of constant coefficients
$E_{k,t}$	Capacity of energy storage unit k at time t
f, h, v, z	Objective functions
$\boldsymbol{H}$	Coefficient matrix corresponding to $\boldsymbol{\theta}$
$\boldsymbol{p}^{vpp}$	Vectors of internal optimization variables for VPPs, including $\boldsymbol{x}$ and $\boldsymbol{y}$
$p_{i,t}^{\mathrm{MT}}$	Active power output of MT unit i at time t
$p_{c,t}^{\mathrm{VPP}}$	Active power output of VPPs at PCC c at time t
$p_{j,t}^{\mathrm{RG}}$	Active power output of renewable energy unit j at time t
$p_{k,t}^{\mathrm{cha}}$	Charging power of energy storage unit k at time t
$p_{k,t}^{\mathrm{dis}}$	Discharging power of energy storage unit k at time t
$p_{ln,t}^{\mathrm{line}}$	Active power transmitted by line ln at time t
$p_{d,t}$	Active power demand of load d at time t
$p_{j,t}^{\mathrm{FRG}}$	Forecast value of active power output of renewable energy unit j at time t
$q_{d,t}$	Reactive power demand of load d at time t
$q_{ln,t}^{\mathrm{line}}$	Reactive power transmitted by line ln at time t
$\boldsymbol{s}$	Non-negative slack variable
U	Dual parameter space
$V_{n,t}$	Square of voltage amplitude at node n
$\boldsymbol{x}$	Vector of decision variables related to unit output and energy storage actions
$\boldsymbol{y}$	Vector of variables for VPPs other than $\boldsymbol{x}$

I. Introduction

WITH developments in communications, artificial intelligence, cloud computing, and other technologies, it is becoming more common for virtual power plants (VPPs) to coordinate and optimize a variety of distributed energy resources (DERs) in a complementary and aggregated manner [1]. In contrast to the traditional microgrid, which emphasizes the local balance between the power generation side and user side and is limited by geographical regions, VPPs overcome the geographical limitations of the scattered DERs and act as independent units that can be scheduled and traded in the energy market [2], [3]. With the continuous expansion of VPPs around the world, the user-side energy storage, electric vehicles, and flexible loads have increasingly contributed to the economic dispatch of power grids, significantly aiding energy transformation and market vitality [4], [5].

VPPs aggregate massive heterogeneous DERs and interact with the main grid at the point of common coupling (PCC) [6]. The interaction between VPPs and the main grid can be regarded as a typical bilevel optimization problem, and traditional research works mainly solve such problems through methods in the following two categories: ① the solution method based on the Karush-Kuhn-Tucker (KKT) conditions, which incorporates the KKT conditions of VPP into the optimization problem of the main grid layer for solution [7]; and ② the iterative method of bilevel model, which follows the iterative "electricity quantity-price" pattern, under which the main grid releases a price signal, the VPP declares the optimal electricity quantity under this price signal, and then the main grid updates the price signal until the electricity quantities declared by the VPP at two adjacent iterations converge within an acceptable error range [8]. However, the above methods have the following drawbacks.

1) The solution method based on KKT conditions requires the VPP operators to submit the full model of VPP to the main grid to determine the precise clearing prices and quantities. This solution method will lead to the disclosure of sensitive parameters of entities in the VPP.

2) The iterative method of bilevel model does not reveal global information on the VPP, which easily leads to oscillation and nonconvergence during the iteration process [9], [10].

In response to the privacy disclosure and oscillating nonconvergence observed in the existing research, many studies have conducted related works. For example, [11] transforms the market equilibrium problem into three sub-models to protect the data privacy of stakeholders and uses an adaptive alternating direction method of multipliers (ADMM) algorithm to reduce the number of iterations. Reference [12] employs a multi-agent reinforcement learning approach to handle the uncertainty and complexity that traditional iterative methods struggle with, achieving the efficient coordination between VPPs and the main grid. In this paper, we aim to achieve the non-iterative market participation of VPPs based on their external characteristics. VPPs declare the bidding functions that can represent their overall flexibility and cost characteristics, which is highly symmetric and compatible with the traditional market system, thus promoting the non-iterative market participation of VPPs.

Therefore, an efficient characterization method for bidding functions of VPPs will have very important practical significance. Reference [13] classifies the aggregation of units in the VPP based on the generation status and proposes an analytical method to estimate the coefficients of the bidding function. This method primarily focuses on economic factors, while physical constraints such as power flow, ramping, and safety are not explicitly considered, which may result in market commitments that could be challenging to implement operationally. Reference [14] estimates the bidding function through the probing method (PM), in which the main grid releases price signals at certain step sizes and the VPP operators determine the optimal power under different price signals, thereby estimating the stepwise bidding curve of VPP. Reference [15] estimates the bidding function for various potential operation states of the VPP based on sampling operational points and proposes a convex piecewise linear fitting method to effectively smooth the bidding function. However, choosing the step size or number of sample points described in [14] and [15] involves a trade-off between the accuracy and computational time. Reference [16] initially determines the transfer region through vertex search and then computes the bidding functions on this region. The unavoidable loss of vertices may lead to a reduction in region accuracy, consequently decreasing the precision of bidding functions. The method proposed in [17] can determine the overall flexibility of VPP, but it neglects the cost characteristics. In summary, the aforementioned methods offer valuable insights and contributions. At the same time, there are a few areas that could benefit from further attention: ① the simultaneous consideration of both the internal safety constraints and cost characteristics of VPP; and ② ensuring an optimal balance between the accuracy and efficiency in solving the bidding function.

Therefore, in this paper, the key innovation for the non-iterative market participation of VPPs is the direct derivation of bidding function for VPPs using a precise and non-approximate method, i.e., the multi-parametric linear programming (MPLP) method. This is a well-established method, which can accurately represent the real bidding functions of VPPs, providing a solid theoretical foundation for non-iterative market participation [18]. For instance, [19] applies MPLP method to study the curve of energy storage value, demonstrating its effectiveness in related applications. However, in such applications, the initial optimization space is typically feasible, often forming a simple geometric shape like a square (e.g., constrained by energy storage capacity) [20]. In contrast, for aggregators like VPPs, the feasible region at PCC is an irregular polyhedron.

This paper aims to minimize the operating cost of VPPs by performing parameter programming for the power exchanged at the PCC. We explore a larger initial parameter space (IPS) that characterizes the bidding function across this parameter space, which includes both feasible and non-feasible regions. Traditional MPLP methods often involve selecting specific parameter points within a broad space to solve the aggregator model [21]. If an optimal solution is found, the analysis then proceeds to calculate the corresponding critical regions (CRs), marginal costs, and bidding function. However, if no optimal solution is found, the parameters must be updated, and the model is solved to explore other potential solutions [22], [23]. For a VPP containing numerous heterogeneous DERs and multi-time-period constraints, the cost of redundant computations due to improper parameter selection can be significant. This highlights the importance of an appropriate strategy to efficiently characterize the precise feasible IPS.

To avoid the increase in time cost due to the redundant solutions and to efficiently characterize the external characteristics of VPPs, this paper characterizes the bidding functions of VPPs based on an improved MPLP method. First, an algorithm for determining the precise IPS is proposed by directly identifying boundaries between feasible and infeasible regions, thereby avoiding redundant solutions in the VPP model during the solving process for CRs. Second, the economic principle of the solution process for CRs is described, and the mapping relationship between the CRs and bidding function of VPPs is analyzed. Subsequently, the analytical form of the CR boundaries is derived, and by solving the dual multipliers corresponding to each CR, an overall bidding function is obtained. Based on the strong duality theory, the bidding function of VPPs is solved in the form of piecewise linear functions. Finally, the effectiveness of the proposed method is validated through case studies based on the IEEE 33-bus and IEEE 123-bus systems. The main contributions of this paper are summarized as follows.

1) The non-iterative market participation of VPPs via bidding function representation is proposed, which is highly symmetric and compatible with existing market pathways. VPPs participate in the electricity market by declaring piecewise linear bidding functions, similar to the technical parameters declared by thermal power plants. The bidding functions reflect the global information of VPPs through low-dimensional parameters while avoiding the disclosure of the internal private information of VPPs.

2) The economic principle underlying the optimal segmentation in the proposed method is revealed, and it is shown that the structure of Lagrange multipliers remains constant within the CR, meaning that the marginal cost of VPPs remains unchanged for any given CR. Based on this characteristic, the piecewise linear mapping relationship between the CR and bidding function is analyzed, followed by the application of strong duality theory to solve the bidding function of VPPs.

3) An algorithm for determining the precise IPS is proposed to address the issue of redundant solutions due to the inaccuracy of IPS. The IPS is usually composed of the transmission limits of tie lines. First, a max-min diagnostic model is proposed as the convergence criterion for precise IPS solution, which is then transformed into a mixed-integer linear programming (MILP) model that can be solved by off-the-shelf solvers. Subsequently, the feasible boundary of IPS is derived, and the infeasible region corresponding to the worst points in the IPS is sequentially trimmed.

The remaining parts of this paper are outlined as follows. Section II aims to clarify the framework for the non-iterative market participation of VPPs. Section III presents an algorithm for determining the precise IPS for VPPs. Section IV derives the bidding function representation for VPPs. Section V validates the effectiveness of the proposed method. Section VI concludes this paper.

II. Framework for Non-iterative Market Participation of VPPs

To address the aforementioned gaps, a framework for the non-iterative market participation of VPPs is constructed. This section aims to provide a unified and stepwise overview of the non-iterative market participation for VPPs, as also illustrated in Fig. 1, clarifying the overall modeling, bidding function derivation, and market clearing pipeline. Specifically, the process proceeds as follows. First, the VPP operator generates the bidding function offline, considering internal safety constraints (steps a1-a4 in Fig. 1). Subsequently, VPPs participate in the electricity market (step a5 in Fig. 1) alongside traditional thermal power plants and centralized renewable energy stations by submitting their bidding functions. Ultimately, the market operator performs a non-iterative centralized clearing based on the submitted bidding information from all market participants, and the clearing results (i. e., allocated quantities and prices) are returned to each participant for execution (step a6 in Fig. 1). For VPPs, upon receiving the cleared electricity quantity, the clearing result is treated as a fixed parameter for the internal optimization, allowing the VPPs to solve for their optimal internal dispatch strategy.

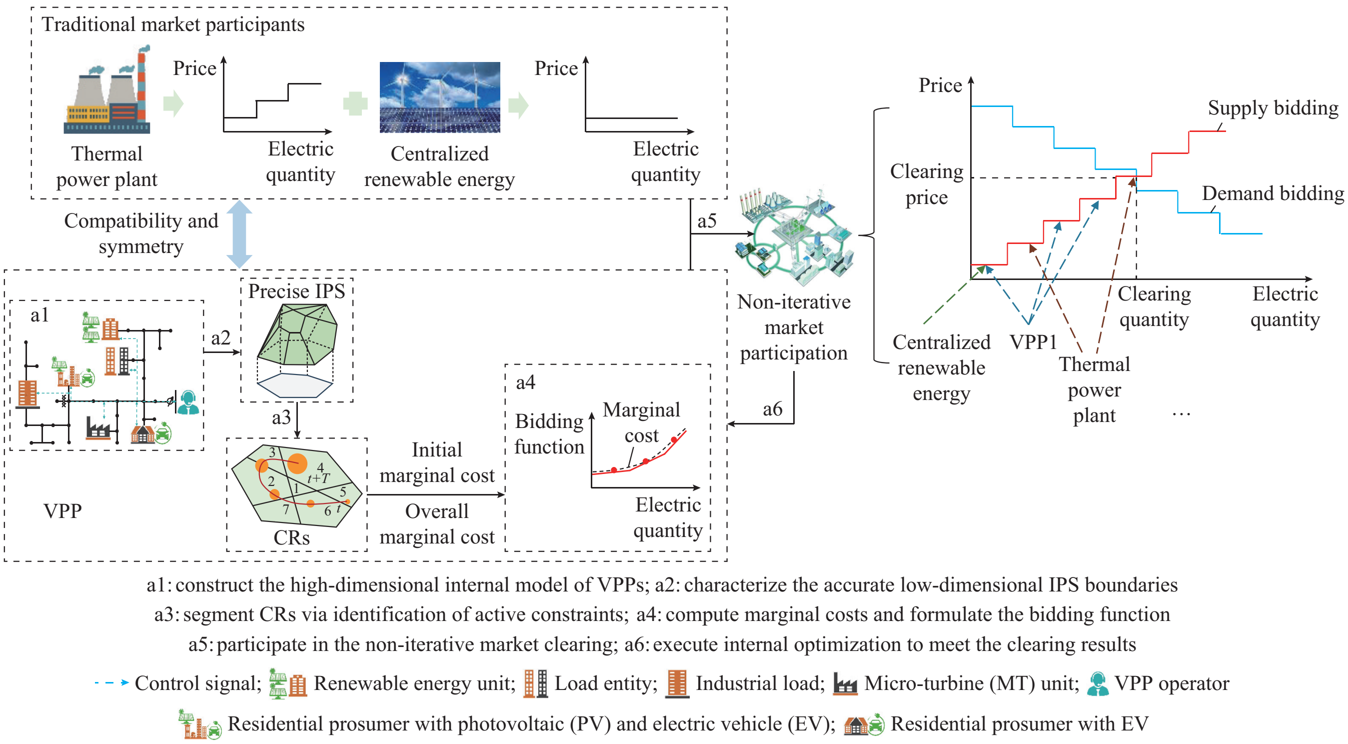

Fig. 1. Illustration for non-iterative market participation of VPPs

The core issue for the non-iterative market participation of VPPs is how to efficiently and accurately solve their bidding functions. To address this issue and enable the effective market participation of VPPs, a corresponding improved MPLP method is proposed. Initially, an algorithm for determining the precise IPS of VPPs is introduced, which achieves rapid IPS solution by sequentially eliminating the non-feasible region corresponding to the worst points. Subsequently, by deriving the boundary equations of CRs based on the effective and ineffective constraints, the IPS is optimally partitioned. Finally, by utilizing the invariance of the dual-multiplier solution structure within the CR, the bidding function is determined based on the theory of strong duality. The non-iterative pathway and algorithm have the following advantages, and will enhance the economic benefits for users.

1) Accurate solution and efficiency enhancement. This paper obtains non-approximate solutions for the bidding function of VPPs, and the delineation of IPS avoids redundant model solutions caused by selecting parameter points outside the feasible region, significantly enhancing the efficiency of processing large-scale VPP models.

2) Privacy protection and global information representation. Bidding functions allow VPPs to avoid submitting their full models to the electricity market, thus protecting the privacy of the internal parameters of VPPs. Additionally, the bidding functions can reflect the overall information of VPPs, enabling non-iterative single clearance.

3) High compatibility with existing market pathways, conforming to path dependence. Similar to traditional thermal power plants, VPPs participate in the electricity market by declaring their bidding functions. This is highly symmetric and compatible with existing market models, avoiding the additional costs associated with market reforms.

It is important to note that the aim of this paper is not to disrupt the existing centralized clearing mechanism, but to design a non-iterative centralized clearing mechanism for emerging market participants like VPPs. In this mechanism, multiple VPPs submit their marginal cost curves alongside traditional market participants without disclosing all private parameters, avoiding issues such as non-convergence and oscillations commonly seen in iterative methods. The market clearing will be carried out centrally based on the marginal pricing mechanism, and the VPPs will be settled according to the clearing price and quantity. This design aligns with the path dependency principle of market reform, minimizing the costs of such reforms. For VPPs, once the allocated market clearing volume is determined, it turns the uncertain parameter θ into a definite clearing quantity. The VPP model then only needs to be solved again given θ to obtain the operational points for its internal entities.

III. Algorithm for Determining Precise IPS for VPPs

A. Problem Description and Parametric Model of VPPs

VPPs can aggregate massive DERs. This paper considers several typical DERs such as energy storage units, MT units, and renewable energy units. This subsection constructs a general model of VPPs [24], [25].

$$f(\boldsymbol{\eta})=\min_{\boldsymbol{p}=[p_{i,t}^{\mathrm{MT}},p_{k,t}^{\mathrm{dis}},p_{k,t}^{\mathrm{cha}}]}\left[\sum_{i\in\phi^{\mathrm{MT}}}\eta_i p_{i,t}^{\mathrm{MT}}+m\sum_{k\in\phi^{\mathrm{BS}}}(p_{k,t}^{\mathrm{dis}}+p_{k,t}^{\mathrm{cha}})\right] \tag{1}$$

$$p_{c,t}^{\mathrm{VPP}}=\left(\sum_{i\in\phi^{\mathrm{MT}}(c)}p_{i,t}^{\mathrm{MT}}+\sum_{j\in\phi^{\mathrm{RG}}(c)}p_{j,t}^{\mathrm{RG}}+\sum_{k\in\phi^{\mathrm{BS}}(c)}p_{k,t}^{\mathrm{dis}}+\sum_{l\in\phi^{\mathrm{N}}}p_{lc,t}^{\mathrm{line}}\right)-\left(\sum_{l\in\phi^{\mathrm{N}}}p_{cl,t}^{\mathrm{line}}+\sum_{k\in\phi^{\mathrm{BS}}(c)}p_{k,t}^{\mathrm{cha}}+\sum_{d\in\phi^{\mathrm{D}}(c)}p_{d,t}\right):\lambda_c(t)\quad\forall c\in\phi^{\mathrm{PCC}},\forall t \tag{2}$$

$$p_{i,\min}^{\mathrm{MT}}\le p_{i,t}^{\mathrm{MT}}\le p_{i,\max}^{\mathrm{MT}}\quad\forall i,\forall t \tag{3}$$

$$-r_i^{\mathrm{MT}}\le p_{i,t}^{\mathrm{MT}}-p_{i,t-1}^{\mathrm{MT}}\le r_i^{\mathrm{MT}}\quad\forall i,\forall t \tag{4}$$

$$0\le p_{j,t}^{\mathrm{RG}}\le p_{j,t}^{\mathrm{FRG}}\quad\forall j,\forall t \tag{5}$$

$$0\le p_{k,t}^{\mathrm{dis}}\le p_{k,\max}^{\mathrm{BS}}:\mu_{k,1}(t),\mu_{k,2}(t)\quad\forall k,\forall t \tag{6}$$

$$0\le p_{k,t}^{\mathrm{cha}}\le p_{k,\max}^{\mathrm{BS}}:\mu_{k,3}(t),\mu_{k,4}(t)\quad\forall k,\forall t \tag{7}$$

$$E_{k,\min}\le E_{k,t}\le E_{k,\max}:\alpha_{k,1}(t),\alpha_{k,2}(t)\quad\forall k,\forall t \tag{8}$$

$$E_{k,t+1}=E_{k,t}+\varepsilon_k^{\mathrm{cha}}p_{k,t}^{\mathrm{cha}}\Delta t-p_{k,t}^{\mathrm{dis}}\Delta t/\varepsilon_k^{\mathrm{dis}}\quad\forall k,\forall t \tag{9}$$

$$E_{k,T}=E_{k,0} \tag{10}$$

$$p_{k,t}^{\mathrm{dis}}p_{k,t}^{\mathrm{cha}}=0\quad\forall k,\forall t \tag{11}$$

$$\sum_{l\in\phi^{\mathrm{N}}}p_{ln,t}^{\mathrm{line}}-\sum_{l\in\phi^{\mathrm{N}}}p_{nl,t}^{\mathrm{line}}+\sum_{i\in\phi^{\mathrm{MT}}(n)}p_{i,t}^{\mathrm{MT}}+\sum_{k\in\phi^{\mathrm{BS}}(n)}p_{k,t}^{\mathrm{dis}}-\sum_{k\in\phi^{\mathrm{BS}}(n)}p_{k,t}^{\mathrm{cha}}=\sum_{d\in\phi^{\mathrm{D}}(n)}p_{d,t}:\lambda_n(t)\quad\forall n\in\phi^{\mathrm{N}}\backslash\phi^{\mathrm{PCC}},\forall t \tag{12}$$

$$\sum_{n\in\phi^{\mathrm{N}}}q_{ln,t}^{\mathrm{line}}-\sum_{n\in\phi^{\mathrm{N}}}q_{nl,t}^{\mathrm{line}}=\sum_{d\in\phi^{\mathrm{D}}(n)}q_{d,t}\quad\forall n\in\phi^{\mathrm{N}}\backslash\phi^{\mathrm{PCC}},\forall t \tag{13}$$

Equation (1) is the objective function for the general model of VPPs that minimizes the total operating cost. Equations (2)-(13) denote the VPP operation constraints. Constraint (2) denotes the power balance limit at the PCC. Constraints (3) and (4) represent the output limit and climb limit of MT unit, respectively. Constraint (5) represents the output limit of renewable energy unit. Constraints (6)-(11) are the operating limits of energy storage units. Constraints (6) and (7) represent the discharging and charging power limits, respectively. Constraints (8)-(10) represent the energy storage capacity limits. Constraint (11) indicates that the energy storage units cannot be charged and discharged at the same time. Equations (12) and (13) represent the active and reactive power balance constraints at nodes other than the PCC, respectively.

Based on the model assumptions and the linearization described in Supplementary Materials A and B, the general model can be written in the compact parametric form, as shown in (14).

$$\begin{cases}\min\limits_{\boldsymbol{x},\boldsymbol{y},\boldsymbol{\theta}}\ f=\boldsymbol{\eta}^{\mathrm{T}}\boldsymbol{x}\\ \text{s.t.}\ \ \boldsymbol{Ax}+\boldsymbol{By}\le\boldsymbol{b}-\boldsymbol{H\theta}\\ \qquad \boldsymbol{x}\ge\boldsymbol{0}\end{cases} \tag{14}$$

For VPPs interacting with the main grid, the proposed method solves the bidding function by exploring the parameter space defined by the power transfer limits of tie lines. The IPS is usually not equivalent to the feasible region of VPPs, and when the fixed parameter points are chosen in the infeasible region of IPS, the redundant solutions will arise, which will be very time-consuming to address. Therefore, the core issue addressed is pre-solving the precise IPS. On one hand, this will avoid computational inefficiencies in solving the bidding function due to inappropriate parameter point selection; on the other hand, the IPS provides a trading safety boundary for VPPs, ensuring that all traded electricity within the IPS can be physically executed. Furthermore, we propose two technical points: ① a diagnostic model of IPS to determine whether the current parameter space is feasible, and ② the precise IPS characterization with an algorithm to identify the boundaries between feasible and infeasible regions.

B. Diagnostic Model of IPS

Suppose that the IPS is denoted as $\Psi=\{\boldsymbol{\theta}|\boldsymbol{K}_0\boldsymbol{\theta}\le\boldsymbol{k}_0\}$. To determine whether all the points in the IPS Ψ are feasible, a max-min diagnostic model is proposed based on the idea of robust optimization as:

$$\begin{cases}\max\limits_{\boldsymbol{\theta}\in\Psi}\ \min\limits_{\boldsymbol{x},\boldsymbol{y},\boldsymbol{s}\ge\boldsymbol{0}}\ h=\boldsymbol{1}^{\mathrm{T}}\boldsymbol{s}\\ \text{s.t.}\ \ \boldsymbol{Ax}+\boldsymbol{By}-\boldsymbol{Is}\le\boldsymbol{b}-\boldsymbol{H\theta}:\boldsymbol{\mu}\end{cases} \tag{15}$$

Theorem 1 Equation (15) defines the distance from the farthest point to the precise IPS (feasible region), which can be used as a criterion for the existence of optimal solutions for all points in the current parameter space Ψ.

Proof If $h=0$, it indicates that there exists a set of optimal solutions of model (14) for all $\boldsymbol{\theta}$ in IPS Ψ; if $h>0$, it indicates that there exists a worst case $\boldsymbol{\theta}_w$ in IPS Ψ that does not satisfy the constraint $\boldsymbol{Ax}+\boldsymbol{By}\le\boldsymbol{b}-\boldsymbol{H\theta}_w$, and a certain degree of relaxation of the VPP security constraints is required for a feasible solution to exist in the worst case $\boldsymbol{\theta}_w$.

However, since the max-min bilayer model is difficult to solve directly with commercial solvers, (15) is transformed into an MILP model, as shown in (16), based on the strong duality theory and the KKT condition. The derivation procedure is shown in Supplementary Material C.

$$\begin{cases}\max\limits_{\boldsymbol{\varphi},\boldsymbol{\lambda},\boldsymbol{\mu}\in U,\boldsymbol{\theta}\in\Psi}\ v=\boldsymbol{\mu}^{\mathrm{T}}\boldsymbol{b}+\boldsymbol{k}_0^{\mathrm{T}}\boldsymbol{\lambda}\\ \text{s.t.}\ \ \boldsymbol{0}\le\boldsymbol{k}_0-\boldsymbol{K}_0\boldsymbol{\theta}\le M\boldsymbol{\varphi}\\ \qquad \boldsymbol{k}_0^{\mathrm{T}}\boldsymbol{\lambda}+\boldsymbol{H}^{\mathrm{T}}\boldsymbol{\mu}=0\\ \qquad \boldsymbol{0}\le\boldsymbol{\lambda}\le M(\boldsymbol{1}-\boldsymbol{\varphi})\end{cases} \tag{16}$$

Since $h=0$ in (15) is equivalent to $v=0$ in (16), the IPS MILP model (16) can be used to determine whether all $\boldsymbol{\theta}$ in

Ψ are feasible. In summary, Theorem 1 provides a convergence criterion for the precise IPS characterization in Section III-C.

C. Precise IPS Characterization

When power is exchanged between the main grid and VPPs within the precise IPS, there is always a dispatch strategy to ensure that the power can be physically traded, meaning that model (14) has an optimal solution. First, the precise IPS at the PCC of VPPs is defined.

Definition 1 The precise IPS Ψ_P is a parameter set such that $\forall \boldsymbol{\theta} \in \Psi_P$, $v=0$; otherwise, $v>0$.

According to Definition 1, the redundant solutions obtained by the traditional MPLP method can be essentially avoided. To solve the precise IPS efficiently, in this paper, the infeasible region corresponding to the worst point in the current parameter space is sequentially removed, and the parameter space is updated until the convergence criterion $v=0$ in (16) is satisfied [26].

Therefore, cutting the infeasible region corresponding to the worst point is the key to the proposed algorithm. Based on the strong duality, $v=0$ in Supplementary Material C (C1) is equivalent to $h=0$ in (15). In addition, (17) holds when $v=0$ (i.e., $\forall \boldsymbol{\theta} \in \Psi$) is feasible.

$$\boldsymbol{\mu}^{\mathrm{T}}(\boldsymbol{b}-\boldsymbol{H\theta})\leq 0 \quad \boldsymbol{\theta}\in\Psi, \boldsymbol{\mu}\in U \tag{17}$$

If $\exists \boldsymbol{\theta}_w \in \Psi$ satisfies $\boldsymbol{\theta}_w \notin \Psi_P$, then (18) holds.

$$\boldsymbol{\mu}_w^{\mathrm{T}}\boldsymbol{b} > \boldsymbol{\mu}_w^{\mathrm{T}}\boldsymbol{H\theta}_w \quad \exists \boldsymbol{\mu}_w \in U \tag{18}$$

Thus, (19) is the boundary separating the feasible region from infeasible one.

$$\boldsymbol{\mu}_w^{\mathrm{T}}\boldsymbol{b} = \boldsymbol{\mu}_w^{\mathrm{T}}\boldsymbol{H\theta} \tag{19}$$

Based on the derivation of feasible boundary, the fast solving process of precise IPS is as follows. First, (16) is solved for IPS Ψ to obtain the value of v, the worst parameter $\boldsymbol{\theta}_w$, and the corresponding dual variable $\boldsymbol{\mu}_w$. If $v=0$, then the current parameter space Ψ is the precise IPS Ψ_P; if $v>0$, then we need to solve the feasible boundary $\boldsymbol{\mu}_w^{\mathrm{T}}\boldsymbol{b} \leq \boldsymbol{\mu}_w^{\mathrm{T}}\boldsymbol{H\theta}$ corresponding to $\boldsymbol{\theta}_w$ according to (19) and update the current parameter space, i.e., $\Psi=\{\boldsymbol{\theta} | \boldsymbol{\theta}\in\Psi, \boldsymbol{\mu}_w^{\mathrm{T}}\boldsymbol{b}\leq\boldsymbol{\mu}_w^{\mathrm{T}}\boldsymbol{H\theta}\}$. Therefore, it is only necessary to solve (16) several times to generate the precise IPS, which effectively reduces the computational burden of the traditional MPLP method due to the improper selection of parameter points in the imprecise IPS.

IV. Bidding Function Representation for VPPs

A. CRs of VPPs

After obtaining the precise IPS of VPPs at the PCC with respect to the traded electricity, the IPS is optimally partitioned to reflect the piecewise linear bidding functions for VPPs, and a number of CRs are obtained. The process of optimizing segmentation in the precise IPS to obtain CRs involves the following economic theorem.

Theorem 2 Within any CR, the marginal cost of VPPs at the PCC is consistent and does not vary with changes in trading parameters.

Proof According to the derivation of the analytic form of the CR boundary outlined below, the corresponding Lagrange multipliers remain invariant within each CR CR_s.

To determine the initial CR CR_0, this paper categorizes the constraints in model (14) into active and non-active constraints based on whether the boundary is reached. First, an arbitrary parameter $\boldsymbol{\theta}_0 \in \Psi_P$ is chosen, and the model (14) given $\boldsymbol{\theta}_0$ is solved to obtain the optimal solutions $\boldsymbol{x}^*$ and $\boldsymbol{y}^*$. The active and nonactive constraints after incorporating $\boldsymbol{\theta}_0$, $\boldsymbol{x}^*$, and $\boldsymbol{y}^*$ are shown in (20) and (21), respectively.

$$\boldsymbol{A}_a\boldsymbol{x}^* + \boldsymbol{B}_a\boldsymbol{y}^* = \boldsymbol{b}_a - \boldsymbol{H}_a\boldsymbol{\theta}_0 \tag{20}$$

$$\boldsymbol{A}_{na}\boldsymbol{x}^* + \boldsymbol{B}_{na}\boldsymbol{y}^* < \boldsymbol{b}_{na} - \boldsymbol{H}_{na}\boldsymbol{\theta}_0 \tag{21}$$

At the same time, (20) and (21) can be rewritten as (22) and (23), respectively, i.e., $\boldsymbol{x}^*$ and $\boldsymbol{y}^*$ are regarded as the expressions $\boldsymbol{x}^*(\boldsymbol{\theta})$ and $\boldsymbol{y}^*(\boldsymbol{\theta})$ with respect to the parameter $\boldsymbol{\theta}$.

$$\boldsymbol{A}_a\boldsymbol{x}^*(\boldsymbol{\theta}) + \boldsymbol{B}_a\boldsymbol{y}^*(\boldsymbol{\theta}) = \boldsymbol{b}_a - \boldsymbol{H}_a\boldsymbol{\theta} \tag{22}$$

$$\boldsymbol{A}_{na}\boldsymbol{x}^*(\boldsymbol{\theta}) + \boldsymbol{B}_{na}\boldsymbol{y}^*(\boldsymbol{\theta}) < \boldsymbol{b}_{na} - \boldsymbol{H}_{na}\boldsymbol{\theta} \tag{23}$$

The parametric expression (24) for the optimization variables $\boldsymbol{x}^*(\boldsymbol{\theta})$ and $\boldsymbol{y}^*(\boldsymbol{\theta})$ is obtained from (22).

$$\begin{bmatrix} \boldsymbol{x}^*(\boldsymbol{\theta}) \\ \boldsymbol{y}^*(\boldsymbol{\theta}) \end{bmatrix} = \boldsymbol{C}_a^{-1}(\boldsymbol{b}_a - \boldsymbol{H}_a\boldsymbol{\theta}) \tag{24}$$

where $\boldsymbol{C}_a = [\boldsymbol{A}_a, \boldsymbol{B}_a]$.

Substituting $\boldsymbol{x}^*(\boldsymbol{\theta})$ and $\boldsymbol{y}^*(\boldsymbol{\theta})$ into (23) and rewriting "$<$" as "$\leq$" yields the parametric expression (25) of the boundary information for CR_0.

$$\boldsymbol{C}_{na}\boldsymbol{C}_a^{-1}(\boldsymbol{b}_a - \boldsymbol{H}_a\boldsymbol{\theta}) \leq \boldsymbol{b}_{na} - \boldsymbol{H}_{na}\boldsymbol{\theta} \tag{25}$$

where $\boldsymbol{C}_{na} = [\boldsymbol{A}_{na}, \boldsymbol{B}_{na}]$.

After obtaining the initial CR, the unexplored precise IPS is updated to $\Psi_P = \Psi_P \backslash CR_s$, and new parameter points are arbitrarily chosen in Ψ_P to determine the corresponding CR via (25). The above procedure is followed to explore the precise IPS Ψ_P until Ψ_P is empty.

B. Bidding Function of VPPs

By the strong duality principle, the optimal values of the primal model and dual model for VPPs are equal, and the optimal operating cost of VPPs can be characterized by the dual model [27], [28]. Therefore, the piecewise linear bidding function of VPPs can be defined as follows.

Definition 2 The piecewise linear bidding function of VPPs with respect to the parameter $\boldsymbol{\theta}$ is equivalent to the objective function of the dual model, reflecting the overall operating costs, marginal costs, and feasible trading region.

The dual model of (14) with dual variable $\boldsymbol{\omega}$ and a given $\boldsymbol{\theta}_0 \in CR_0$ is shown in (26).

$$\begin{cases} \max\limits_{\boldsymbol{\omega}} z = (\boldsymbol{b} - \boldsymbol{H\theta}_0)^{\mathrm{T}}\boldsymbol{\omega} \\ \text{s.t. } \boldsymbol{A}^{\mathrm{T}}\boldsymbol{\omega} \leq \boldsymbol{\eta} \\ \quad\;\; \boldsymbol{B}^{\mathrm{T}}\boldsymbol{\omega} = 0 \end{cases} \tag{26}$$

Solving (26) yields the optimal dual variable $\boldsymbol{\omega}_0$ corresponding to $\boldsymbol{\theta}_0$ and the optimal operating cost. Since the optimal dual multiplier remains constant within CR_0, it is always $\boldsymbol{\omega}_0$. Hence, the operating cost of VPPs on CR_0 is $z_0^* = (\boldsymbol{b} - \boldsymbol{H\theta})^{\mathrm{T}}\boldsymbol{\omega}_0, \boldsymbol{\theta} \in CR_0$. Extending this to CR_s, the piecewise linear bidding function z^* for VPP is given by (27).

$$z^*=\begin{cases}(\boldsymbol{b}-\boldsymbol{H\theta})^{\mathrm{T}}\boldsymbol{\omega}_1 & \boldsymbol{\theta}\in CR_1\\(\boldsymbol{b}-\boldsymbol{H\theta})^{\mathrm{T}}\boldsymbol{\omega}_2 & \boldsymbol{\theta}\in CR_2\\ \vdots & \\(\boldsymbol{b}-\boldsymbol{H\theta})^{\mathrm{T}}\boldsymbol{\omega}_s & \boldsymbol{\theta}\in CR_s\end{cases} \tag{27}$$

where $CR_1\cup CR_2\cup\ldots\cup CR_n=\Psi_P$.

C. Additional Remarks

To avoid the selection of initial parameters $\boldsymbol{\theta}_0$ at the intersection of multiple CRs, a judgment model for this phenomenon and an improvement method are provided. A Gaussian transformation is applied to the active constraint (20) corresponding to the initially given parameter $\boldsymbol{\theta}_0$, resulting in (28).

$$\begin{bmatrix}\boldsymbol{R} & \boldsymbol{D}\\ \boldsymbol{0} & \boldsymbol{S}\end{bmatrix}\begin{bmatrix}\boldsymbol{p}^{vpp}\\ \boldsymbol{\theta}\end{bmatrix}=\begin{bmatrix}\boldsymbol{a}\\ \boldsymbol{c}\end{bmatrix} \tag{28}$$

where $\boldsymbol{R}$, $\boldsymbol{D}$, and $\boldsymbol{S}$ are the coefficient matrices after Gaussian transformation for (20); and $\boldsymbol{a}$ and $\boldsymbol{c}$ are the constant terms after Gaussian transformation for (20). When the rank of $\boldsymbol{S}$ is zero, there is no equation in the active constraints that is only related to the parameter, and the initial parameter is not at the boundary of CRs. Conversely, if the rank of $\boldsymbol{S}$ is nonzero, the initial parameter is chosen at the junction of multiple CRs.

For the case of a matrix $\boldsymbol{S}$ with nonzero rank, given any $\boldsymbol{\rho}$ satisfying (29), we have $\boldsymbol{\theta}_1=\boldsymbol{\theta}_0+\boldsymbol{\rho}$, and $\boldsymbol{\theta}_1$ remains within the feasible region and will not be selected at the CR boundary.

$$\|\boldsymbol{\rho}\|_2<\min_r\left\{|\boldsymbol{K}_r\boldsymbol{\theta}_0-\boldsymbol{k}_r|/\sqrt{\boldsymbol{K}_r\boldsymbol{K}_r^{\mathrm{T}}}\right\} \tag{29}$$

where $\|\boldsymbol{\rho}\|_2$ is the Euclidean parameter of $\boldsymbol{\rho}$; and $|\boldsymbol{K}_r\boldsymbol{\theta}_0-\boldsymbol{k}_r|/\sqrt{\boldsymbol{K}_r\boldsymbol{K}_r^{\mathrm{T}}}$ is the distance of the initial parameter from the boundary of CR_s, and $\boldsymbol{K}_r$ and $\boldsymbol{k}_r$ are the coefficient vectors of the linear terms and right-hand-side constants of the r^{th} CR boundary hyperplane, respectively.

In summary, the process of the proposed method for deriving the bidding function of VPPs is shown in Algorithm 1.

It mainly consists of two phases: Phase I determines the precise IPS, i.e., stages 1-8, and Phase II is for constructing the bidding function of VPPs, i.e., stages 9-18. The pruned precise IPS Ψ_P, obtained at stage 8, is directly used as the initial search space for CR partitioning at stage 10, thereby reducing the redundant computations commonly found in traditional MPLP method.

Algorithm 1: process of proposed method for deriving bidding function of VPPs

Input: cost coefficient $\boldsymbol{\eta}$ and constraint coefficients $\boldsymbol{A}$, $\boldsymbol{B}$, $\boldsymbol{H}$, and $\boldsymbol{b}$ for model (14)

1. Initialize the IPS $\Psi=\{\boldsymbol{\theta}|\boldsymbol{K}_0\boldsymbol{\theta}\le\boldsymbol{k}_0\}$
2. Solving (16) yields v and $\boldsymbol{\mu}_w$
3. **while** $v>0$ in (16)
4. Solve the feasible boundary $\boldsymbol{\mu}_w^{\mathrm{T}}\boldsymbol{b}\le\boldsymbol{\mu}_w^{\mathrm{T}}\boldsymbol{H\theta}$ corresponding to $\boldsymbol{\theta}_w$ in the current parameter space Ψ
5. Update the current parameter space $\Psi=\{\boldsymbol{\theta}|\boldsymbol{\theta}\in\Psi,\boldsymbol{\mu}_w^{\mathrm{T}}\boldsymbol{b}\le\boldsymbol{\mu}_w^{\mathrm{T}}\boldsymbol{H\theta}\}$
6. Solve (16) under the updated Ψ and obtain v and $\boldsymbol{\mu}_w$
7. **end while**
8. Obtain the precise IPS $\Psi_P=\Psi$
9. Initialize the index s of CR and bidding function, i.e., $s=0$
10. **while** $\Psi_P\neq\varnothing$
11. $s=s+1$
12. Arbitrarily select a given parameter point $\boldsymbol{\theta}_0$ and solve (14) to obtain $\boldsymbol{x}^*$ and $\boldsymbol{y}^*$
13. CR_s is obtained through (25)
14. Marginal cost is obtained through dual variables at the PCC
15. Bidding function on CR_s is obtained through (27)
16. Update the unexplored precise IPS $\Psi_P=\Psi_P\backslash CR_s$
17. **end while**
18. **Output**: CRs and bidding function of VPP

V. Case Studies

The effectiveness of the proposed method is verified based on the modified IEEE 33-bus and IEEE 123-bus systems. The proposed method can accurately solve the bidding functions of VPPs and characterize the global information of VPPs. The bidding functions of VPPs with multiple time periods can be used for intraday rolling clearing. The platform for analyzing the proposed algorithm is MATLAB R2018a, and the optimization calculation tool is IBM ILOG CPLEX 12.6.

A. Modified IEEE 33-bus System

In the modified IEEE 33-bus system, the VPPs have a total active load demand of 31.9 MW and a total reactive load demand of 11.5 Mvar. The generation resources of VPPs include three MT units and four PV field stations. The installed capacity of each MT unit is 7 MW, the climb power limit is 0.7 MW, the generation cost coefficients of the three MT units are 14.1, 23.0, and 9.0 \$/MW, and these three MT units are located at buses 1, 7, and 18, respectively. The four PV field stations are located at buses 7, 12, 11, and 19, respectively, and the predicted PV outputs are shown in Table I [29]. Due to the limitations of personal computer processing power, this paper considers the coupling of five time points, i.e., 05:00, 09:00, 13:00, 17:00, and 21:00.

TABLE I
PREDICTED PV OUTPUT AT EACH TYPICAL MOMENT

Time	$p_{1,t}^{\mathrm{FRG}}$ (MW)	$p_{2,t}^{\mathrm{FRG}}$ (MW)	$p_{3,t}^{\mathrm{FRG}}$ (MW)	$p_{4,t}^{\mathrm{FRG}}$ (MW)
05:00	0	0	0	0
09:00	1.59	2.52	0.13	0.08
13:00	2.52	4.85	1.09	1.04
17:00	2.00	4.03	1.35	1.15
21:00	0.04	0.10	0.02	0.02

B. Bidding Function Considering Active Power Interactions

The PCC of VPPs is bus 1, and the internal power flow limits are all 0.7 MW. Considering the active power (P) interactions, the bidding function and stepwise marginal cost at 13:00 are shown in Fig. 2. The analytical form of the bidding function with different power flow limits is shown in Table II, where θ equals P. In Fig. 2(a), different colors of lines correspond to different ranges of P.

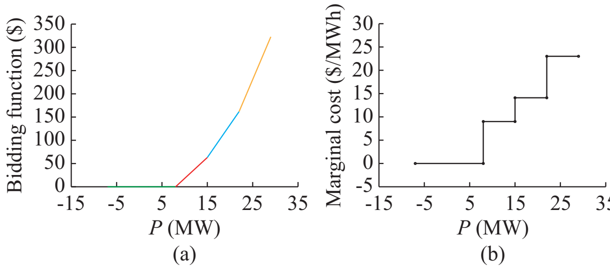

Fig. 2. Bidding function and stepwise marginal cost considering active power interactions at 13:00. (a) Bidding function. (b) Stepwise marginal cost.

TABLE II
ANALYTICAL FORM OF BIDDING FUNCTION WITH DIFFERENT POWER FLOW LIMITS

Power flow limit (MW)	Bidding function ($)	Range of θ (MW)	Marginal cost ($/MW)	Feasible region (MW)
0.7	0.00	[−7.0, 8.0]	0	[−7.00, 29.00]
	$9.00\theta-72.00$	[8.0, 15.0]	9.00	
	$14.10\theta-148.50$	[15.0, 22.0]	14.10	
	$23.00\theta-343.30$	[22.0, 29.0]	23.00	
0.1	0.00	[−1.0, 7.0]	0	[−1.00, 27.42]
	$9.00\theta-63.00$	[7.0, 14.0]	9.00	
	$14.10\theta-134.40$	[14.0, 20.9]	14.10	
	$23.00\theta-320.19$	[20.9, 26.3]	23.00	
	$26.02\theta-399.73$	[26.3, 26.6]	26.02	
	$28.91\theta-476.83$	[26.6, 27.3]	28.91	
	$99.26\theta-2399.15$	[27.3, 27.4]	99.26	

When $-7.0\ \text{MW}\leq\theta\leq 8.0\ \text{MW}$, the value of the bidding function for VPPs is 0. This is because: ① this paper does not consider the cost of purchasing power from the main grid; and ② the marginal cost of renewable energy generation is zero. The VPPs can achieve non-iterative clearing by declaring external parameters such as its bidding function and feasible region.

Parameters such as the internal power flow limits of VPPs and the installed capacity and climb power limits of generation units all affect the external characteristics of VPP. Taking the power flow limit as an example, when it is 0.7 MW, the marginal cost on each CR is consistent with the generation cost of unit, and the corresponding power range is consistent with the installed capacity of unit, which is 7 MW. However, when the power flow limit becomes tighter, i.e., 0.1 MW, the bidding function is shown in Fig. 3.

Compared with the case where the power flow limit is 0.7 MW, setting the power flow limit to 0.1 MW reduces the feasible region of the VPP trading. Meanwhile, higher marginal costs (26.02, 28.91, and 99.26 $/MW) than the generation cost of unit are observed, which are attributed to transmission line blockage.

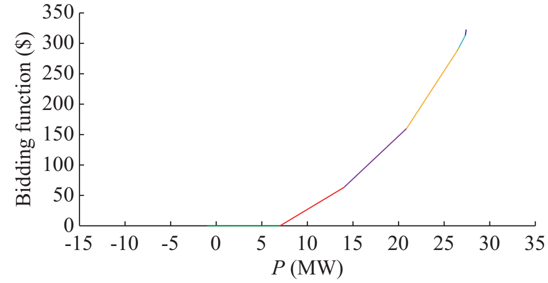

Fig. 3. Bidding function with power flow limits of 0.1 MW.

C. Bidding Function Considering Active and Reactive Power Interactions

In specific scenarios, VPPs need to engage in reactive power (Q) interactions with the main grid, which also impacts the costs of VPPs.

Therefore, this paper introduces reactive power interaction on the basis of active power interaction, depicting the feasible region for reactive and active power and the bidding function. On one hand, this paper can provide theoretical guidance on bidding for future VPPs participating in multi-type ancillary service markets; on the other hand, the proposed method is applicable for depicting high-dimensional and complex bidding functions. The precise IPS and CRs of VPPs considering the active and reactive power interactions at 13:00 are shown in Fig. 4(a) and (b), respectively.

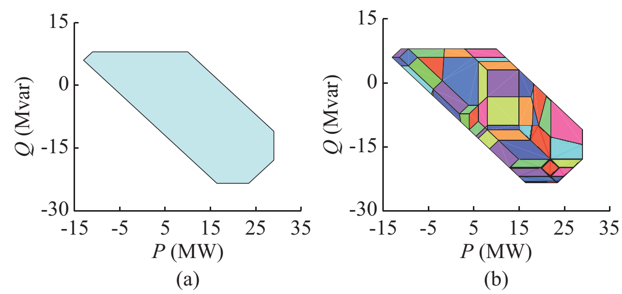

Fig. 4. Precise IPS and CRs of VPPs considering active and reactive power interactions at 13:00. (a) Precise IPS. (b) CRs.

As shown in Fig. 4(a), on one hand, the precise IPS provides a clear security boundary for VPP trading; on the other hand, the precise IPS provided for subsequent parametric programming can effectively avoid redundant solution caused by the imprecise one. Figure 4(b) shows the visualization result of CRs for the IPS, where each color block corresponds to a CR, in which the parameters correspond to the same set of active and reactive constraints and the Lagrange multipliers are the same.

Figure 5 shows the bidding function of VPPs considering active and reactive power interactions at 13:00, which also includes the marginal cost information. Each color block corresponds to a CR and represents a segment in the piecewise bidding function.

At the same time, there exist several sets of CRs for which the value of bidding function is zero. This is also because the cost of purchasing power is not considered and the cost of renewable energy output is zero.

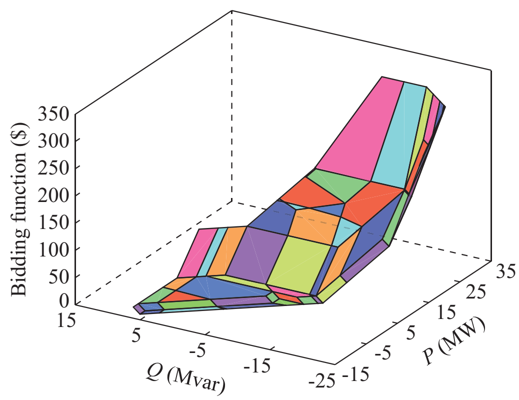

Fig. 5. Bidding function of VPPs considering active and reactive power interactions at 13:00.

The size of this region is related to the level of renewable energy output at 13:00 and the VPP demand. This paper considers the coupling of multi-period constraints for VPPs. The precise multi-period IPS for the five typical time points is shown in Fig. 6(a). Figure 6(b)-(e) displays the CRs and low-dimensional bidding functions at 05:00, 09:00, 17:00, and 21:00, considering time-coupling constraints, respectively.

As the results show, the feasible region and bidding function of VPPs vary significantly across different time points. This is due to the spatiotemporal correlations of distributed entities such as renewable energy units, energy storage units, and thermal power units. Therefore, it is essential to fully consider the time-coupling constraints during the solution process. In the case study of this paper, we assume that the initial operation state of VPPs is known and proceeds to solve the subsequent IPS and bidding function while considering time-coupling constraints. In practice, the proposed method can be applied to intraday rolling scheduling, where the bidding function for decision period is generated by considering the operation state of VPPs in the previous period and incorporating the coupling constraints from the remaining future periods. The bidding function for the intraday decision periods is then rolled out and used for bidding.

Figure 7 illustrates the coupling relationship between the feasible active power outputs at PCC for 05:00 (P_5) and those for 09:00, 13:00, and 17:00 (P_9, P_{13}, and P_{17}). As the time intervals increase, the coupling relationship gradually diminishes. When it degenerates into a standard rectangle, it indicates that the operation states of the two time points do not affect each other. Therefore, before the VPPs solve their bidding function and participates in the intraday rolling scheduling, the VPP aggregator can understand the coupling relationships between different time points based on VPP parameters. When solving the bidding function, only the coupling constraints from future time point that will affect the current time point need to be considered. This will significantly reduce the computational complexity of solving the bidding function and enhance the practical applicability.

D. Efficiency Verification

To verify the effectiveness of the proposed method for characterizing the bidding functions of VPPs, the solution accuracy and efficiency of the proposed method (M1), the traditional MPLP method (M2), and the PM (M3) are compared.

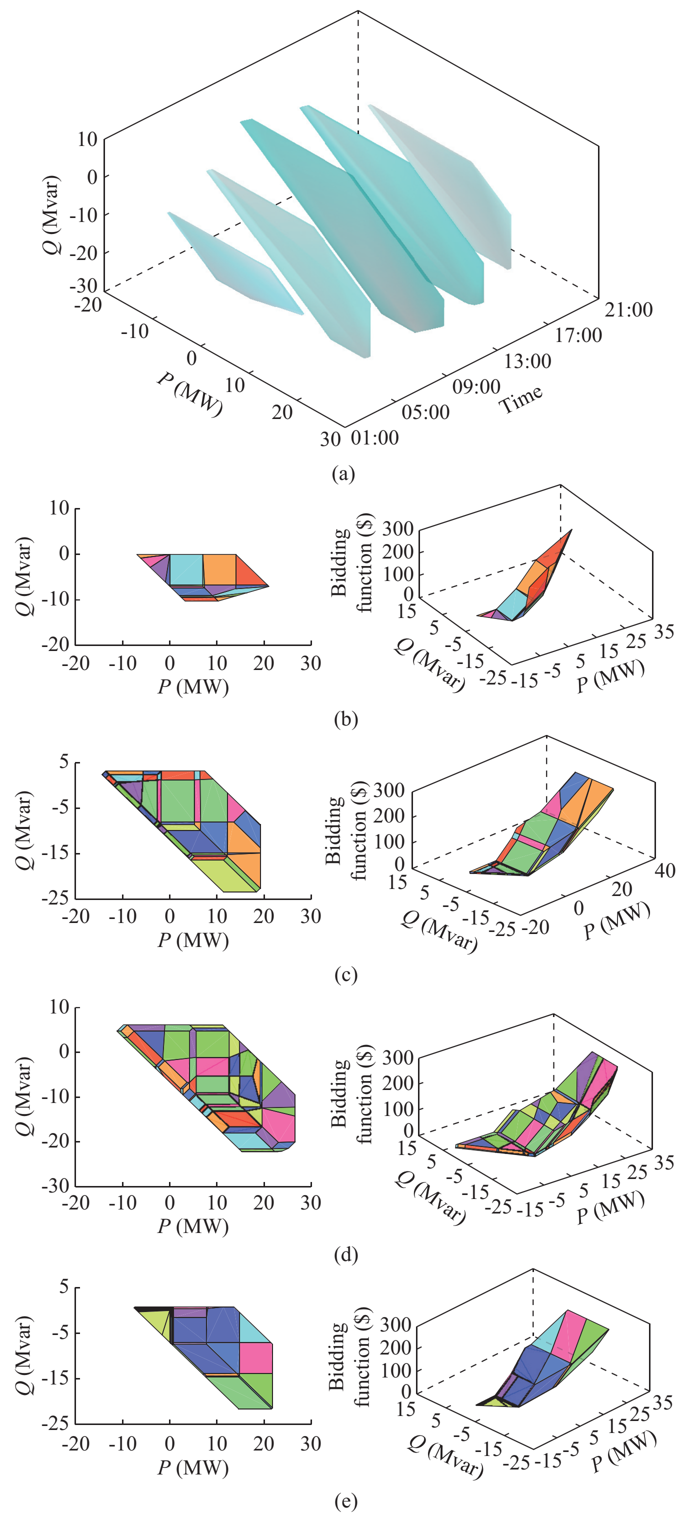

Fig. 6. Multi-period IPS and bidding function of VPPs for five typical time points. (a) Precise multi-period IPS of VPPs for five typical time points. (b) CRs and bidding function at 05:00. (c) CRs and bidding function at 09:00. (d) CRs and bidding function at 17:00. (e) CRs and bidding function at 21:00.

The average solution time for the bidding function is shown in Table III. In Table III, Case 1 represents solving the bidding function considering the active power interactions; and Case 2 represents solving the bidding function considering the active and reactive power interactions.

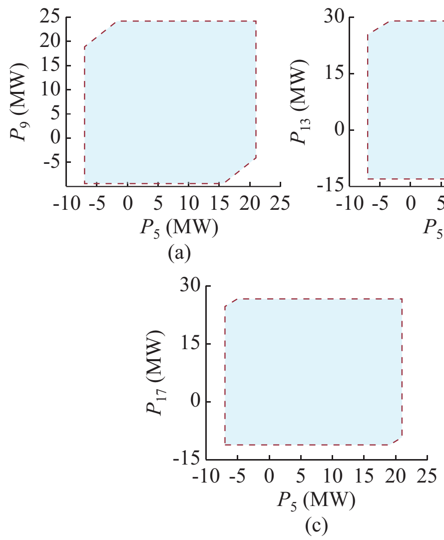

Fig. 7. Coupling relationship between feasible active power outputs at PCC for 05:00 and those for 09:00, 13:00, and 17:00. (a) 05:00 and 09:00. (b) 05:00 and 13:00. (c) 05:00 and 17:00.

TABLE III
AVERAGE SOLUTION TIME FOR BIDDING FUNCTION

Case	Time of M1 (s)	Time of M2 (s)	M3		
			Time (s)	Probing number	Error (%)
Case 1	39.88	43.49	13.89	4	29.21
			42.68	16	10.15
			209.41	64	5.04
Case 2	519.63	1685.32	365.14	4	36.52
			725.52	16	15.59
			3285.64	64	9.37

In addition, the error in the case study is obtained by comparing samples of the bidding function generated with M2.

In M1, the precise IPS is solved first and then the parametric programming is carried out in this space to solve the bidding functions. In M2, the parametric programming is carried out directly in the parameter space consisting of the transmission power constraints of the VPP-main grid tie-lines. M3 is carried out through different price signals released by the main grid, where the VPP operator optimally solves the corresponding price boundaries to obtain the optimal interaction electricity, and the stepped price curve of VPPs is estimated after many interactions.

From the results in Table III, it can be observed that in Case 1, where the parameter space is 1-dimensional, M1 has almost the same solution time as M2. In Case 2, where the parameter space is 2-dimensional, M1 is significantly faster than M2. This is because as the parameter space dimension increases, the number of redundant solutions in the infeasible region that may arise in M2 increases dramatically. Moreover, the results show that it is difficult for M3 to characterize the precise external properties of VPPs, and the increasing computational cost is needed to improve the accuracy during the probing process. M3 will lead to a large amount of communication and arithmetic power consumption in pursuit of accuracy. Moreover, M2 may result in some redundancy in the division of CRs, i. e., two regions may share the same marginal cost. As shown in Table III, the impact of this redundancy on computational efficiency is acceptable. In the practical bidding, the VPPs can further merge the solved bidding function before submitting it to the market operator.

E. Modified IEEE 123-bus System

In the modified IEEE 123-bus system, VPPs have four MT units, one energy storage unit, and five PV stations. The active and reactive load demands are 52.8 MW and 23.0 Mvar, respectively.

The multi-period bidding function of VPPs considering the time-coupling constraints is shown in Fig. 8. The bidding function can be expressed as $a_{s,t}\theta+b_{s,t}$, where $a_{s,t}$ is the marginal cost of VPPs, and $b_{s,t}$ is the constant term of the bidding function over the s^{th} CR. The bidding function and marginal costs for multiple time points show the generation and operation status of VPPs at different time points. For example, at 13:00, the VPPs have a longer phase of zero marginal cost and a larger feasible region of traded power because of the abundant PV resources, while the highest marginal cost is also obtained. In contrast, at 01:00, since there are no PV resources, as long as VPPs send active power, their operating and marginal costs are positive, and their feasible region of traded power decreases. Due to the limited computational power of personal computers, in the IEEE 123-bus system, only the results of projecting onto the active power parameter are considered. This is because projecting onto both the active and reactive power dimensions and considering time coupling for more than six time periods makes it difficult to solve the bidding function within one hour.

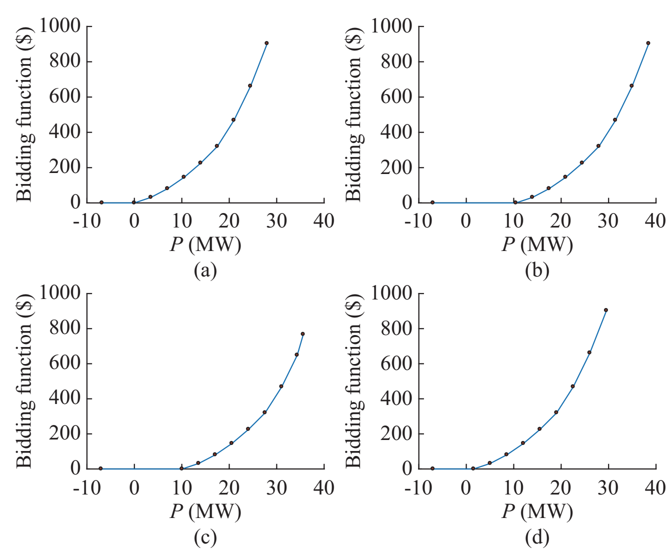

Fig. 8. Multi-period bidding function of VPPs considering time-coupling constraints. (a) 01:00. (b) 09:00. (c) 13:00. (d) 21:00.

The coupling relationship of the traded VPP power at three typical time points (denoted as P_1, P_2, and P_3) in feasible region is shown in Fig. 9. If the time-coupling constraints are not considered, the feasible region for active power coupling between different time points should be a regular cube rather than an irregular polytope.

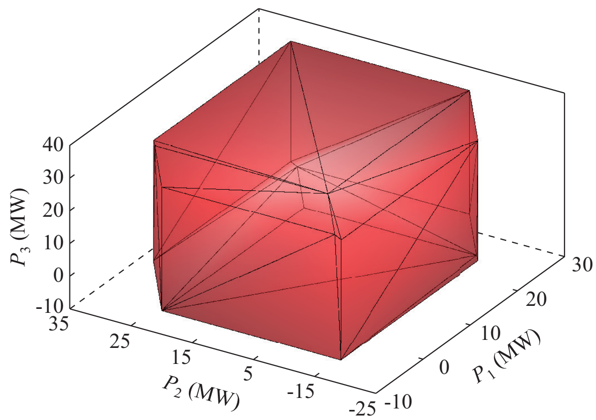

Fig. 9. Coupling relationship of traded active power at three typical time points in feasible region.

F. Sensitivity Analysis of Complexity and Scale

The sensitivity analysis of complexity and scale is conducted on the modified IEEE 123-bus system. The temporal dimension under different numbers of coupling periods and the growth in the number of DERs are both considered, as shown in Fig. 10.

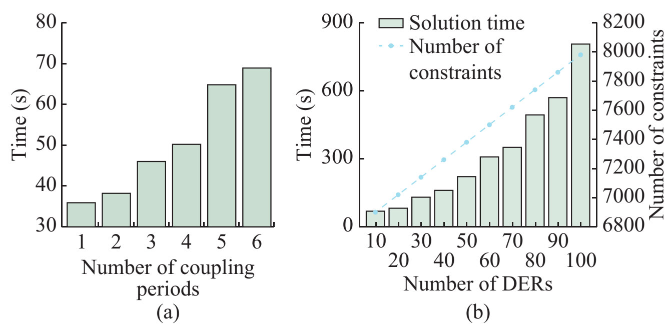

Fig. 10. Sensitivity analysis result of number of coupling periods and DERs. (a) Number of coupling periods. (b) Number of DERs.

The analysis results are as follows.

1) From the temporal dimension perspective, when projecting onto a single-dimensional parameter (i.e., active power), the solution time gradually increases with the number of coupling periods. Despite considering multi-period coupling, the bidding function for the single-dimensional parameter can still be efficiently solved. However, for the bidding function considering multi-dimensional parameters, using two-dimensional active and reactive power parameters as examples, as the number of coupling periods increases from 1 to 3, the solution time for the bidding function for a specific period is 58.23, 135.65, and 2812.14 s, respectively, eventually exceeding 1 hour. Therefore, to some extent, the impact of the projection dimension on computational complexity is greater than that of time-coupling constraints.

2) For the number of DERs, when it is increased from 10 to 100 (a tenfold increase) while considering the coupling of six time periods, the changes in the number of constraints and solution time are analyzed. As the number of DERs increases, both the solution time and the model complexity gradually increase. Notably, this is significantly related to the proportion of DERs with the time-coupling relationships among DERs. This paper increases the number of DERs proportionally. If only non-time-coupled resources such as PVs and wind turbines are increased, the increase in solution time is relatively small. For example, if the number of DERs remains at 100, the numbers of MT units and energy storage units remain unchanged, and only PVs are added, the solution time is 427.3 s, which is significantly less than the 805.8 s depicted in Fig. 10(b).

VI. Conclusion

In this paper, a non-iterative market participation of VPPs is constructed via their bidding function representation, which reflects the global internal information of VPPs through low-dimensional parameters. The problems of privacy disclosure and oscillating nonconvergence for the traditional MPLP method are effectively solved. To solve the bidding functions of VPPs efficiently, this paper addresses the problem in the traditional MPLP method that the redundant solutions cannot be avoided due to the inaccuracy of IPS. An algorithm for determining the precise IPS is proposed based on removing the infeasible region corresponding to the worst parameter; an analytical characterization method for CRs is derived; and the economic properties of the optimal segmentation are obtained, based on which the bidding functions are solved. The analysis results based on the modified IEEE 33-bus and IEEE 123-bus systems show that the proposed method can efficiently represent the bidding functions of VPPs at the PCC and avoid disclosure of the private information of VPPs.

In our future work, there are two valuable research directions worthy of further exploration: ① avoiding redundant cuts for the critical region will further enhance the applicability of the algorithm in this paper; and ② efficient clearing methods between multiple VPPs should be further investigated.

References

[1] J. Wang, L. Chen, Z. Tan *et al*., "Inherent spatiotemporal uncertainty of renewable power in China," *Nature Communications*, vol. 14, no. 1, p. 5379, Sept. 2023.

[2] G. Mohy-ud-din, K. M. Muttaqi, and D. Sutanto, "A cooperative energy transaction model for VPP integrated renewable energy hubs in deregulated electricity markets," *IEEE Transactions on Industry Applications*, vol. 58, no. 6, pp. 7776-7791, Nov.-Dec. 2022.

[3] Z. Yi, Z. Zhao, Y. Xu *et al*., "Market clearing model for energy-constrained virtual power plants with uncertainty based on distributionally robust chance-constrained optimization," *Journal of Modern Power Systems and Clean Energy*, vol. 13, no. 6, pp. 2157-2167, Nov. 2025.

[4] Z. Ding, J. Wang, Y. Song *et al*., "Tracking the carbon footprint of global generative artificial intelligence," *The Innovation*, vol. 6, no. 5, p. 100866, May 2025.

[5] W. Liao, D. Yang, Q. Liu *et al*., "Data-driven reactive power optimization of distribution networks via graph attention networks," *Journal of Modern Power Systems and Clean Energy*, vol. 12, no. 3, pp. 874-885, May 2024.

[6] C. Feng, Y. Wang, X. Wang *et al*., "Device access optimization for virtual power plants in heterogeneous networks," *IEEE Transactions on Smart Grid*, vol. 13, no. 2, pp. 1478-1489, Mar. 2022.

[7] W. Zheng and D. J. Hill, "Incentive-based coordination mechanism for

distributed operation of integrated electricity and heat systems," *Applied Energy*, vol. 285, p. 116373, Mar. 2021.
[8] E. G. Kardakos, C. K. Simoglou, and A. G. Bakirtzis, "Optimal offering strategy of a virtual power plant: a stochastic bi-level approach," *IEEE Transactions on Smart Grid*, vol. 7, no. 2, pp. 794-806, Apr. 2015.
[9] Z. Zhang, N. Zhang, E. Du *et al*.,"Modeling and integrating frequency security constraints in generation portfolio optimization for low-inertia grids," *Journal of Modern Power Systems and Clean Energy*, vol. 13, no. 6, pp. 1854-1870, Nov. 2025.
[10] N. Yang, Z. Dong, L. Wu *et al*., "A comprehensive review of security-constrained unit commitment," *Journal of Modern Power Systems and Clean Energy*, vol. 10, no. 3, pp. 562-576, Jul. 2022.
[11] T. Jiang, C. Wu, T. Huang *et al*., "Optimal market participation of VPPs in TSO-DSO coordinated energy and flexibility markets," *Applied Energy*, vol. 360, p. 122730, Apr. 2024.
[12] J. Yao, W. Hao, Z. Meng *et al*., "Adaptive multi-agent reinforcement learning for dynamic pricing and distributed energy management in virtual power plant networks," *Journal of Electronic Science and Technology*, vol. 23, no. 1, p. 100290, Mar. 2025.
[13] M. Qu, T. Ding, W. Wei *et al*., "An analytical method for generation unit aggregation in virtual power plants," *IEEE Transactions on Smart Grid*, vol. 11, no. 6, pp. 5466-5469, Nov. 2020.
[14] T. W. Haring, J. L. Mathieu, and G. Andersson, "Comparing centralized and decentralized contract design enabling direct load control for reserves," *IEEE Transactions on Power Systems*, vol. 31, no. 3, pp. 2044-2054, May 2016.
[15] S. Wang, W. Wu, Q. Chen *et al*., "Stochastic flexibility evaluation for virtual power plant by aggregating distributed energy resources," *CSEE Journal of Power and Energy Systems*, vol. 10, no. 3, pp. 988-999, May 2024.
[16] W. Lin and C. Zhao, "Cost functions over feasible power transfer regions of virtual power plants," *IEEE Systems Journal*, vol. 17, no. 2, pp. 2950-2960, Aug. 2022.
[17] T. Zhang, J. Wang, Q. Xia *et al*., "Extracting umbrella constraint-based representation of local electricity markets," *IEEE Transactions on Smart Grid*, vol. 14, no. 2, pp. 1632-1641, Mar. 2023.
[18] Z. Guo, W. Wei, L. Chen *et al*., "Impact of energy storage on renewable energy utilization: a geometric description," *IEEE Transactions on Sustainable Energy*, vol. 12, no. 2, pp. 874-885, Sept. 2020.
[19] Z. Guo, W. Wei, L. Chen *et al*., "Economic value of energy storages in unit commitment with renewables and its implication on storage sizing," *IEEE Transactions on Sustainable Energy*, vol. 12, no. 4, pp. 2219-2229, Oct. 2021.
[20] Y. Wu, J. Wang, Y. Song *et al*., "Resilience-oriented valuation for energy storage amidst extreme events," *Chinese Journal of Electrical Engineering*, vol. 9, no. 3, pp. 15-25, Sept. 2023.
[21] A. Falsone, F. Bianchi, and M. Prandini, "Dealing with infeasibility in multi-parametric programming for application to explicit model predictive control," *Automatica*, vol. 157, p. 111279, Nov. 2023.
[22] W. Lin, Z. Yang, J. Yu *et al*., "Determination of transfer capacity region of Tie lines in electricity markets: theory and analysis," *Applied Energy*, vol. 239, pp. 1441-1458, Apr. 2019.
[23] S. Wu, J. Lin, J. Li *et al*., "Multi-timescale trading strategy for renewable power to ammonia virtual power plant in the electricity, hydrogen, and ammonia markets," *IEEE Transactions on Energy Markets, Policy and Regulation*, vol. 1, no. 4, pp. 322-335, Dec. 2023.
[24] W. Huang, E. Du, T. Capuder *et al*., "Reliability and vulnerability assessment of multi-energy systems: an energy hub based method," *IEEE Transactions on Power Systems*, vol. 36, no. 5, pp. 3948-3959, Feb. 2021.
[25] W. Zheng, D. J. Hill, and W. Wu, "A multi-parametric programming based analytic method to compute consumer offer curve for reserves," *Journal of Modern Power Systems and Clean Energy*, vol. 10, no. 2, pp. 542-546, Mar. 2022.
[26] D. Pozo, "Convex hull formulations for linear modeling of energy storage systems," *IEEE Transactions on Power Systems*, vol. 38, no. 6, pp. 5934-5936, Nov. 2023.
[27] Y. Song, J. Wang, T. Zhang *et al*., "Characterizing spatiotemporal-coupled resilience of power systems via a security region-based method," *CSEE Journal of Power and Energy Systems*, doi: 10.17775/CSEEJPES.2024.06560
[28] K. Wang, J. Wang, Y. Song *et al*., "Resilience-oriented power system planning amidst extreme events via vehicle-to-grid coordination," *International Journal of Electrical Power & Energy Systems*, vol. 172, p. 111202, Nov. 2025.
[29] Y. Song, T. Zhang, and J. Wang, "Unveiling the segmented patterns of energy storage via parametric grid-resilience value curve," in *Proceedings of 2025 IEEE Industry Applications Society Annual Meeting*, Taipei, China, Jun. 2025, pp. 1-5.

Yiyang Song is currently pursuing the Ph. D. degree at the Department of Electrical and Electronic Engineering, The University of Hong Kong, Hong Kong, China. His research interests include virtual power plant, electricity market, and application of large language model in power system.

Jianxiao Wang received the B. S. and Ph. D. degrees in electrical engineering from Tsinghua University, Beijing, China, in 2014 and 2019, respectively. He was a Visiting Student Researcher at Stanford University, Stanford, USA. He is currently an Associate Professor with Peking University, Beijing, China. He received IEEE PES Outstanding Volunteer Award in 2021. He is leading Excellent Young Scholar Fund of National Science Foundation of China, and Young Scientist Program of National Key Research and Development Program of China. He is a Youth Editor of Cell The Innovation and an Associate Editor of IEEE Transactions on Industry Applications. His research interests include data analytics and optimization for smart grid and energy storage.

Yi Wang received the B. S. degree from Huazhong University of Science and Technology, Wuhan, China, in 2014, and the Ph. D. degree from Tsinghua University, Beijing, China, in 2019. He was a Visiting Student with the University of Washington, Washington DC, USA, from March 2017 to April 2018. He served as a Postdoctoral Researcher in the Power Systems Laboratory, ETH Zurich, Zurich, Switzerland, from February 2019 to August 2021. He is currently an Assistant Professor with the Department of Electrical and Electronic Engineering, The University of Hong Kong, Hong Kong, China. His research interests include data analytics in smart grid, energy forecasting, multi-energy system, Internet-of-Things, and cyber-physical-social energy system.